1.48 and 1.84 μm thulium emissions in monoclinic KGd(WO4)2 single crystals

F. Güell, Jna. Gavaldà, R. Solé, M. Aguiló, F. Díaz et al.

Citation: J. Appl. Phys. **95**, 919 (2004); doi: 10.1063/1.1633985

View online: http://dx.doi.org/10.1063/1.1633985

View Table of Contents: http://jap.aip.org/resource/1/JAPIAU/v95/i3

Published by the American Institute of Physics.

1.48 and 1.84 μm thulium emissions in monoclinic $KGd(WO_4)_2$ single crystals

F. Güell, Jna. Gavaldà, R. Solé, M. Aguiló, and F. Díaz
Física i Cristal·lografia de Materials (FiCMA), Universitat Rovira i Virgili, 43005 Tarragona, Spain

M. Galan
Monocrom SL, Poligon Industrial Les Roquetes, Nau 1, 08800 Vilanova i la Geltrú, Barcelona, Spain

J. Massons[a)]
Física i Cristal·lografia de Materials (FiCMA), Universitat Rovira i Virgili, 43005 Tarragona, Spain

(Received 14 August 2003; accepted 27 October 2003)

By exciting at 788 nm, we have characterized the near infrared emissions of trivalent thulium ions in monoclinic $KGd(WO_4)_2$ single crystals at 1.48 and 1.84 μm as a function of dopant concentration from 0.1% to 10% and temperature from 10 K to room temperature. We used the reciprocity method to calculate the maximum emission cross-section of 3.0×10^{-20} cm^2 at 1.838 μm for the polarization parallel to the N_m principal optical direction. These results agrees well with the experimental data. Experimental decay times of the $^3H_4\rightarrow{}^3F_4$ and $^3F_4\rightarrow{}^3H_6$ transitions have been measured as a function of thulium concentration. © *2004 American Institute of Physics*. [DOI: 10.1063/1.1633985]

I. INTRODUCTION

$KGd(WO_4)_2$ single crystals (hereafter KGW) are very attractive materials as laser hosts. Their monoclinic structure provides an appreciable optical anisotropy suitable for obtaining polarized laser radiation. They are easily grown and Gd^{3+} can be efficiently substituted by Tm^{3+} ions.[1] Thulium lasers are sources of light in the near infrared region, around 1.5 μm, on the $^3H_4\rightarrow{}^3F_4$ transition, which is very interesting for telecommunications purposes, and around 1.8 μm, on the $^3F_4\rightarrow{}^3H_6$ transition, which is used in remote sensing of the atmosphere (LIDAR devices) and in developing medical laser technologies. Interest in thulium-doped crystals is motivated by progress in powerful, well-developed AlGaAs laser diodes, which are well suited for optical pumping at around 800 nm into the $^3H_4$ energy level of thulium ions.

The 1.5 μm transition takes place between the $^3H_4$ and the $^3F_4$ excited energy levels of thulium. This transition is self-terminating because the lifetime of the $^3F_4$ terminal level is longer than that of the $^3H_4$ emitting level.[2,3] This creates a detrimental bottlenecking effect because it is difficult to achieve the population inversion between the $^3H_4$ and $^3F_4$ states without depopulating the lower state. On the other hand, this transition has two competitive transitions, the $^3H_4\rightarrow{}^3H_6$ transition, around 800 nm, and the $^3H_4\rightarrow{}^3H_5$ transition, around 2.3 μm. Both situations are complicating the realization of a highly efficient optical amplification at 1.5 μm. In 1983, Antipenko *et al.*[4] demonstrated for the first time laser oscillations from the $^3H_4\rightarrow{}^3F_4$ transition in $BaYb_2F_8$ and $LiYbF_4$ single crystals.

The 1.8 μm transition occurs between the lowest excited state $^3F_4$ and the ground state $^3H_6$ of thulium ions. The first report of continuous wave room temperature (hereafter RT) laser operation of the $^3F_4\rightarrow{}^3H_6$ transition of Tm^{3+}, pumped by 785 nm laser diode, was in YAG by Kintz *et al.*[5] in 1988. However, the narrow absorption band of thulium in YAG (and YLF) made diode pumping difficult. This laser operation was also achieved in monoclinic tungstates, in two sensitized compounds $KY(WO_4)_2:Er^{3+}$, Tm^{3+} and $KGW:Er^{3+}$, Yb^{3+}, Tm^{3+} single crystals at 1.92 and 1.93 μm, respectively, by Kaminskii *et al.*[6] in 1997 at cryogenic temperatures (110 K), and in thulium-doped $KY(WO_4)_2$ single crystals at 1.95 μm, by Bagaev *et al.*[7] in 2000 at RT. They found that the thulium concentration must be high enough to ensure efficient pumping, but low enough to minimize concentration quenching effects due to cross-relaxation type ($^3H_4+{}^3H_6\rightarrow{}^3F_4+{}^3F_4$) and nonradiative energy transfer between active ions.

Thulium ions present another near infrared emission around 2.3 μm, on the $^3H_4\rightarrow{}^3H_5$ transition, for which laser action has already been achieved.[8] This wavelength has applications in gas detection, medicine and remote sensing.

In this paper, we have characterized the near infrared emissions at 1.48 and 1.84 μm of thulium-doped KGW single crystals by pumping at 788 nm. We analyzed luminescence as a function of thulium concentration and temperature. The reciprocity method has been used to calculate the 1.84 μm emission cross-section from the absorption cross-section and compared with the experimental results. The decay times corresponding to the emitting levels $^3H_4$ and $^3F_4$ were measured at several thulium concentrations.

II. EXPERIMENTAL

The single crystals were grown by the top-seeded-solution growth (TSSG) slow-cooling technique.[9] Electron probe micro analysis (EPMA) results showed that the dopant concentrations of the samples were 6.9×10^{19}, 16.1×10^{19},

[a)]Author to whom correspondence should be addressed. Electronic mail: massons@correu.urv.es

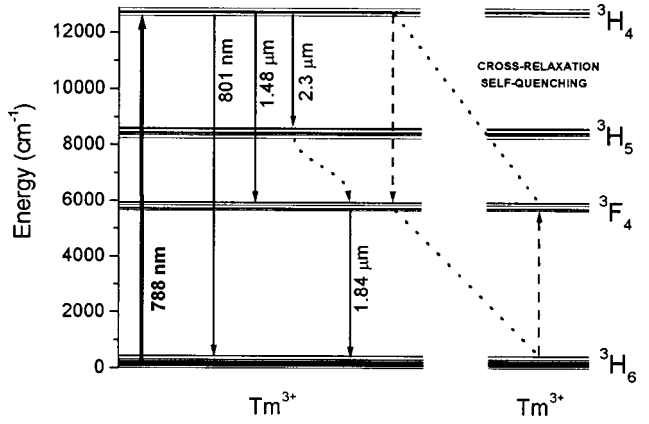

FIG. 1. Partial energy level diagram of Tm^{3+}-doped KGW single crystals.

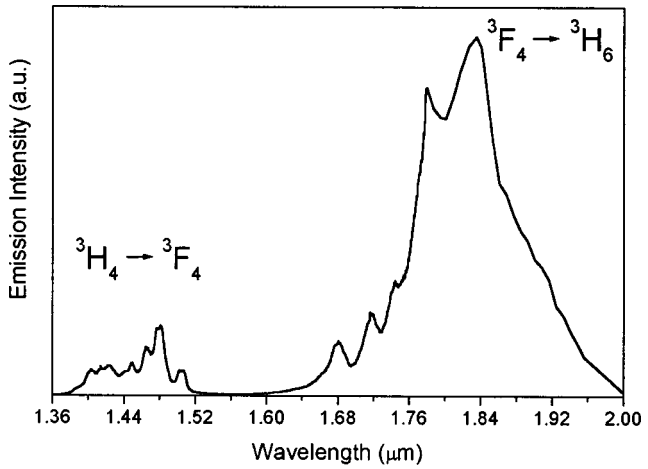

FIG. 2. Room temperature near infrared emissions spectrum of a 3% thulium-doped KGW sample by exciting at 788 nm.

25.7×10^{19}, 37.8×10^{19}, and 55.0×10^{19} at/cm^3, which correspond to molar percentages of Tm_2O_3 substituting Gd_2O_3 in the solution of 1%, 3%, 5%, 7.5%, and 10%, respectively. We also obtained single crystals with 0.1% but the detection limit of EPMA is above this concentration.

For the absorption and emission experiments, the sample was a prism of $KGd_{0.974}Tm_{0.026}(WO_4)_2$ with a thulium concentration of 16.1×10^{19} at/cm^3 (3% in the solution), because this provided enough signal-to-noise ratio without saturating the detector. We cut and polished the prism with the faces perpendicular to the three principal optical directions, to a thickness of 1.11 mm for the N_p and N_m, and 1.47 mm for the N_g. Optical absorption spectra were measured with a VARIAN CARY-5E-UV-VIS-NIR 500Scan Spectrophotometer. Emission spectra were obtained with an Optical Parametrical Oscillator, VEGA 100, pumped by the third harmonic of a Q-switched YAG:Nd laser (pulse duration: 7 ns, repetition rate: 10 Hz), SAGA 120, from B.M. Industries. Fluorescence was dispersed through a HR460 Jobin Yvon-Spex monochromator (focal length: 460 mm, f/5.3, spectral resolution: 0.05 nm). The gratings used were a 600 grooves/mm grating blazed at 1 μm and a 300 grooves/mm grating blazed at 2 μm. The detectors applied were Hamamatsu: R5509-72 NIR photomultiplier, G5832-03 InGaAs PIN photodiode, and a P5968-100 InSb photovoltaic. These were connected to a Perkin Elmer 7265DSP lock-in amplifier. Lifetime measurements were taken at various thulium concentrations. Time decay curves were recorded using a Tektronix TDS-714 digital oscilloscope. For low temperature emission measurements, the samples were mounted into a closed cycle helium cryostat OXFORD CCC1104.

III. LUMINESCENCE RESULTS

For the luminescence studies, we recorded excitation spectra monitoring 1.48 μm while exciting the $^3H_4$ energy level between 760 and 820 nm. The maximum emission intensity was obtained by pumping at 788 nm. At this pump wavelength, the electronic population was excited from the ground state $^3H_6$ to the $^3H_4$ energy level, as illustrated in Fig. 1. The $^3H_4$ energy level relaxes to the three lower states $^3H_6$, $^3F_4$ and $^3H_5$, generating the 801 nm, 1.48 μm and 2.3 μm emissions, respectively. The $^3H_5$ energy level is rapidly depopulated by multiphonon processes to the $^3F_4$ state, which radiatively decays to the $^3H_6$ ground state, generating the 1.84 μm emission. We observed no radiative emission from the $^3H_5$ energy level. The $^3F_4$ energy level is also populated via cross-relaxation mechanisms through the phonon-assisted self-quenching process[10] $^3H_4+{}^3H_6\rightarrow{}^3F_4+{}^3F_4$ (see Fig. 1). The effectivity of this quenching process increases with higher thulium concentrations. Note that we have two steady-state population inversions on the $^3H_4\rightarrow{}^3F_4$ and $^3F_4\rightarrow{}^3H_6$ transitions.

We found that the intensity of these emissions was strongly affected by the concentration of thulium. Maximum emission intensity was in samples containing 3% thulium. The increase in emission intensity due to increases in the thulium concentration was limited by quenching phenomena. Figure 2 shows the RT emission spectra for a 3% sample of the 1.48 and 1.84 μm emissions, corresponding to the $^3H_4\rightarrow{}^3F_4$ and $^3F_4\rightarrow{}^3H_6$ transitions, respectively, after pumping at 788 nm. At thulium concentrations from 1% to 10%, the 1.84 μm emission intensity was stronger than the 1.48 μm emission intensity, while at 0.1% it is the opposite. This can be explained because of the $^3F_4$ state is highly affected by cross-relaxation mechanisms ($^3H_4+{}^3H_6\rightarrow{}^3F_4+{}^3F_4$), which favored the $^3F_4\rightarrow{}^3H_6$ transition.

Moreover, we analyzed the evolution with temperature of these emission channels. From the low temperature spectra we corroborated the corresponding energies of the Stark sublevels of the $^3F_4$ and $^3H_6$ states obtained in previous studies.[11,12] Figure 3 shows the temperature dependency of the 1.48 μm emission spectrum from 10 K to RT. We labeled the n Stark levels, increasing from 0 to n in energy, n' for the upper level and n for the lower level. At 10 K the spectrum shows eight peaks at 1.440, 1.450, 1.452, 1.457, 1.482, 1.500, 1.502 and 1.508 μm, which correspond to the electronic transitions $^3H_4(0')\rightarrow{}^3F_4(0)$, $^3H_4(0')\rightarrow{}^3F_4(1)$, $^3H_4(0')\rightarrow{}^3F_4(2)$, $^3H_4(0')\rightarrow{}^3F_4(3)$, $^3H_4(0')\rightarrow{}^3F_4(4)$, $^3H_4(0')\rightarrow{}^3F_4(5)$, $^3H_4(0')\rightarrow{}^3F_4(6)$ and $^3H_4(0')\rightarrow{}^3F_4(8)$, respectively. The emission peak between $^3H_4(0')\rightarrow{}^3F_4(7)$ overlaps the $^3H_4(0')\rightarrow{}^3F_4(6)$ transition and is located at 1.504 μm. We observed that the emission intensities de-

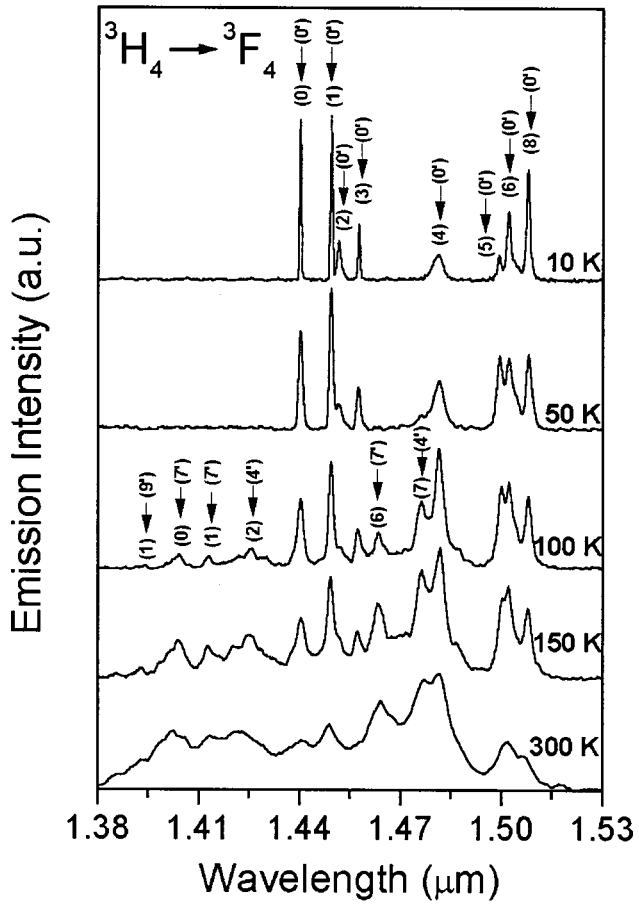

FIG. 3. Temperature evolution of the 1.48 μm emission of thulium in KGW.

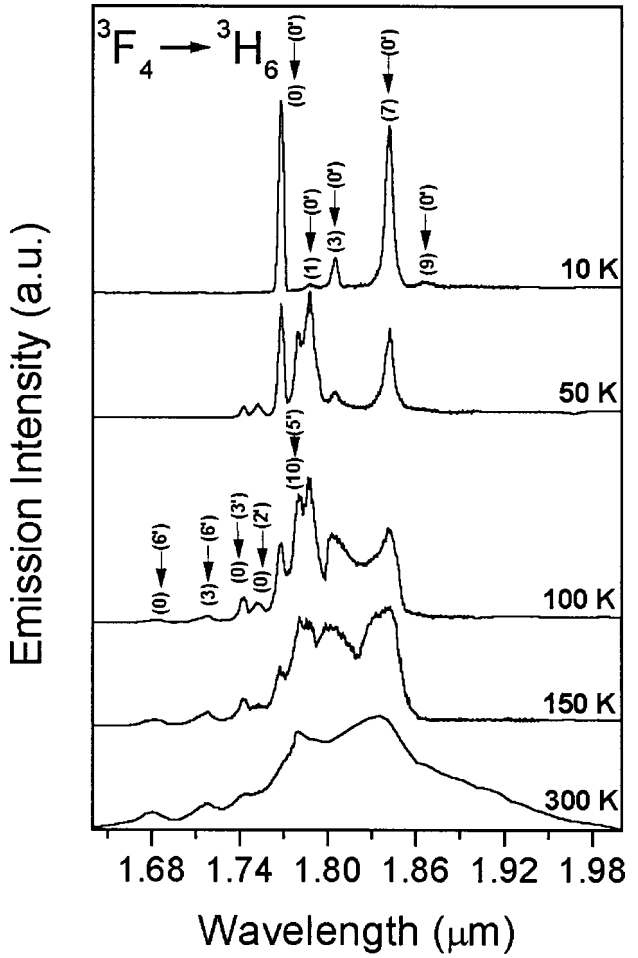

FIG. 4. Temperature evolution of the 1.84 μm emission of thulium in KGW.

creased when the temperature increased. This is due to the thermal population of the sublevels, so at 100 K some new peaks appeared that corresponded to the electronic transitions $^3H_4(9') \rightarrow {}^3F_4(1)$, $^3H_4(7') \rightarrow {}^3F_4(0)$, $^3H_4(7') \rightarrow {}^3F_4(1)$, $^3H_4(4') \rightarrow {}^3F_4(2)$, $^3H_4(7') \rightarrow {}^3F_4(6)$ and $^3H_4(4') \rightarrow {}^3F_4(7)$, which were located at 1.393, 1.404, 1.413, 1.425, 1.463 and 1.476 μm, respectively. In Fig. 4 we present the temperature evolution from 10 K to RT of the 1.84 μm emission. We observed five peaks at 1.770, 1.791, 1.808, 1.842 and 1.869 μm at 10 K, which correspond to the electronic transitions $^3F_4(0') \rightarrow {}^3H_6(0)$, $^3F_4(0') \rightarrow {}^3H_6(1)$, $^3F_4(0') \rightarrow {}^3H_6(3)$, $^3F_4(0') \rightarrow {}^3H_6(7)$ and $^3F_4(0') \rightarrow {}^3H_6(9)$, respectively. These Stark sublevels of the ground state $^3H_6$ are located at 0, 69, 119, 223 and 300 cm^{-1}, respectively. The thermal behavior of the 1.84 μm emission is similar to that of the 1.48 μm emission. At 100 K new peaks appeared at 1.684, 1.718, 1.744, 1.753 and 1.781 μm, corresponding to the $^3F_4(6') \rightarrow {}^3H_6(0)$, $^3F_4(6') \rightarrow {}^3H_6(3)$, $^3F_4(3') \rightarrow {}^3H_6(0)$, $^3F_4(2') \rightarrow {}^3H_6(0)$ and $^3F_4(5') \rightarrow {}^3H_6(10)$ transitions, respectively.

To quantify the 1.84 μm emission, we used the reciprocity method (RM)[13] to determine the emission cross-section of the $^3F_4 \rightarrow {}^3H_6$ transition. The emission cross-section (σ_{em}) is calculated from the absorption cross-section (σ_{abs}) and the splitting of the energy levels using the following equation:

$$\sigma_{em}(\nu) = \sigma_{abs}(\nu) \frac{Z_l}{Z_u} \exp\left[\frac{(E_{ZL} - h\nu)}{k_B T}\right], \tag{1}$$

where Z_l and Z_u are the partition functions, and E_{zl} is the zero-line or energy separation between the lowest energy sublevels of the ground state (lower) and the first excited state (upper), respectively. The partition functions are calculated from

$$Z = \sum_k d_k \exp\left[\frac{-E_k}{k_B T}\right], \tag{2}$$

where d_k and the E_k are the degeneracies and the energies, respectively, of each sublevel of the upper and lower energy levels involved. In our case the ratio Z_l/Z_u was 1.21 and E_{zl} was 5651 cm^{-1}. Figure 5 shows the calculated emission and experimental absorption cross-section for the three polarizations of the $^3F_4 \rightarrow {}^3H_6$ transition at RT in the 1.55–2.00 μm range. The maximum emission cross-sections are 3.0×10^{-20} cm^2 for the polarization parallel to the N_m principal optical direction at 1.838 μm and 1.9×10^{-20} cm^2 for the polarization parallel to the N_p principal optical direction at 1.756 μm. Figure 5 shows that these spectra exhibit the characteristic optical anisotropy of the host KGW, where the spectrum for the $E \| N_m$ polarization is the most intense resulting in the highest possibility to obtain polarized stimulated emission. Figure 6 compares the experimental unpolarized 1.84 μm emission at RT with the spectrum calculated with the reciprocity method, taking into account the unpolar-

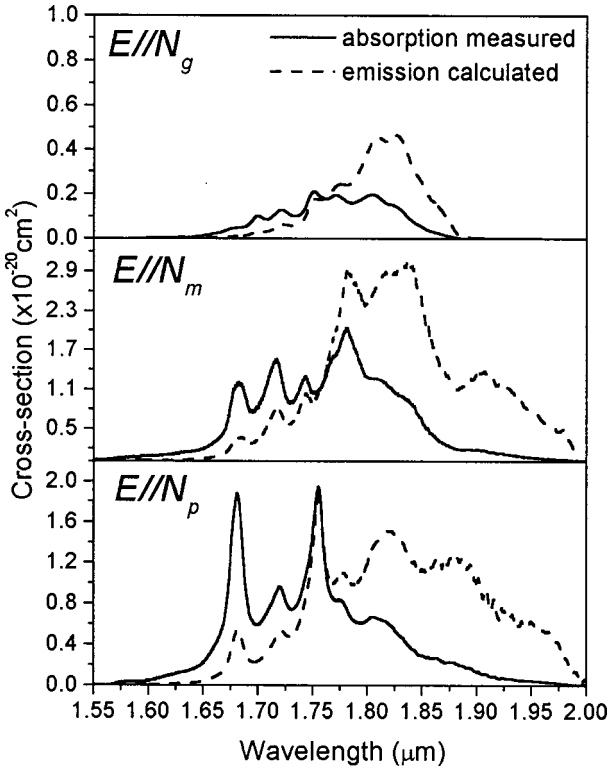

FIG. 5. Calculated emission cross-section at RT for the three polarizations of the $^3F_4 \rightarrow {}^3H_6$ transition by the reciprocity method.

ized absorption spectrum at RT. We rescaled the experimental spectrum to match the calculated spectra and compare its shape. There is good agreement between them, but the peak that appears in the calculated emission spectrum around 1.9 μm was not found experimentally. It was produced by the numerical method that amplifies the absorption spectrum at long wavelengths. These absorption and emission cross-section spectra will be useful for designing and modeling CW and pulsed lasers. In Table I we report a bibliographic study and our results of the emission cross-section of the

TABLE I. Summary of some published values of the $^3F_4 \rightarrow {}^3H_6$ emission cross-section and radiative lifetime of the $^3F_4$ state in different hosts.

Host:[Tm^{3+}]	$\sigma_{em}(\times 10^{-20}$ cm^2)	$\tau(^3F_4(\mu s))$	Reference
$KGd(WO_4)_2$:Tm (3%)	3.0	1760	
$KY(WO_4)_2$:Tm (15%)	1.90	1470	7
YVO_4:Tm (5%)	1.60	800	15
$YAlO_3$:Tm (6%)	0.50	12000	16
KY_3F_{10}:Tm (1%)	0.40	15400	17
$SrGdGa_3O_7$:Tm (3%)	0.39	4700	18
$LiYF_4$:Tm (1%)	0.33	13000	19
LaF_3:Tm (0.1%)	0.25	11000	19
$Y_3Al_5O_{12}$:Tm (1%)	0.22	8500	19

$^3F_4 \rightarrow {}^3H_6$ thulium transition obtained in other hosts. As can be seen in Table I, the emission cross-section of thulium in KGW is higher than in the other crystals.

The $^3F_4 \rightarrow {}^3H_6$ transition corresponds to a quasi-three-level laser scheme in which the lower level is thermally populated at RT. This results in considerable reabsorption and an increased threshold for laser operation. Reducing reabsorption and maintaining efficient absorption of the pump light is one of the key issues in the design of thulium-doped laser systems on this transition. The reabsorption processes of the 1.84 μm emission by resonant transitions occurs when absorption and emission overlapping is important. As a first approximation, the threshold for light amplification is achieved when the emitted light counterbalances the absorption losses. If β is the population inversion rate, this condition can be described as $\sigma_{gain}=\beta\cdot\sigma_{em}-(1-\beta)\cdot\sigma_{abs}$, where σ_{gain} is the effective emission cross-section. Figures 7 and 8 show this condition for $E\|N_m$ and $E\|N_p$ polarizations in the 1.55–2.0 μm spectral region for the $^3F_4 \rightarrow {}^3H_6$ transition. The population inversion rate needed to achieve amplification is expected to be higher than 0.05. For a population inversion level of 0.2, the gain is produced in the 1.85–2.0 μm region. The higher energy limit of this interval increased when the population inversion level was increased, reaching up to 1.75 μm for a population inversion level of 0.5. For this level the maximum gain cross-section value was 1.06×10^{-20} cm^2 at 1.84 μm for $E\|N_m$ and 0.53×10^{-20} cm^2 at

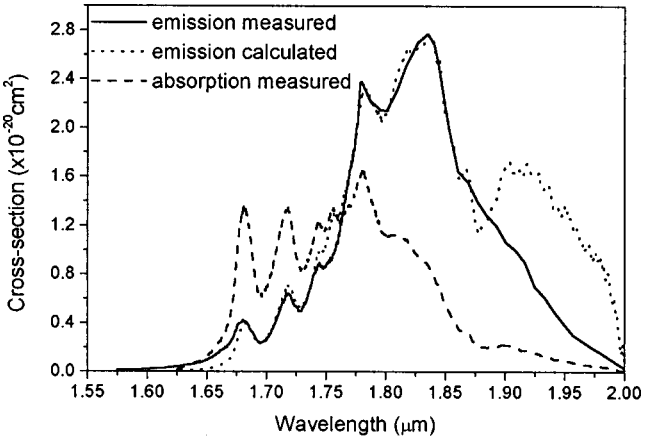

FIG. 6. Comparison of the unpolarized emission cross-section calculated by the reciprocity method and the experimental emission spectrum obtained at RT of the $^3F_4 \rightarrow {}^3H_6$ transition.

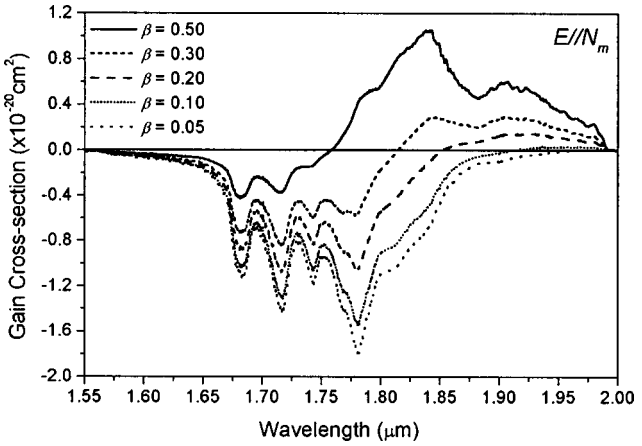

FIG. 7. Gain cross-section of the 1.84 μm emission at RT for the $E\|N_m$ polarization at several inversion population rates.

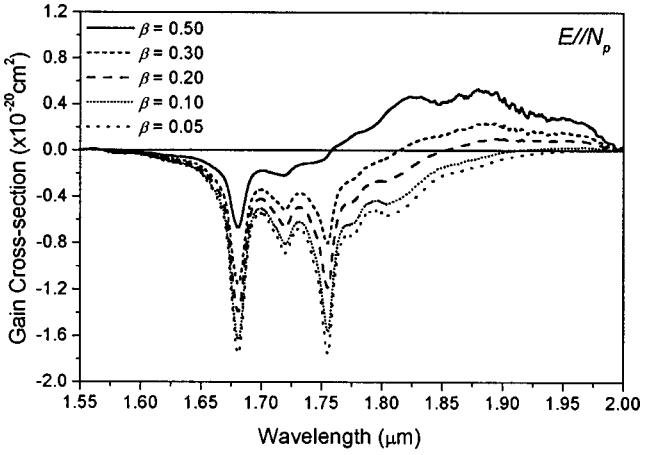

FIG. 8. Gain cross-section of the 1.84 μm emission at RT for the $E\|N_p$ polarization at several inversion population rates.

1.88 μm for $E\|N_p$. At this point we expect to find light amplification in future laser experiments for this emission.

Finally, we investigated the fluorescence dynamics of the $^3H_4$ and $^3F_4$ emitting levels as a function of thulium concentration ranging from 0.1% to 10%. The experimental lifetime of the $^3H_4$ state decreased strongly as the thulium concentration increased (see Table II). This is explained by the very efficient energy transfer mechanisms between thulium ions. At higher thulium concentrations the quenching phenomenon takes place because the Tm–Tm distances decrease. In contrast to the $^3H_4$ relaxation, the decay times of the transition from the $^3F_4$ level were constant for all thulium concentrations (see Table II). The fact that the lifetime of the $^3F_4$ state does not depend on the concentration of thulium is due to two different mechanisms. The first one is the reabsorption effect, or the so-called self-trapping[14] process between $^3F_4 \rightarrow {}^3H_6$ resonant transitions that produces radiative energy transfer between thulium ions, and the second is a repopulation of the emitting level via the $^3H_4 + {}^3H_6 \rightarrow {}^3F_4 + {}^3F_4$ self-quenching cross-relaxation mechanism. This transfer is phonon-assisted since the energy gaps $^3H_4 \rightarrow {}^3F_4 = 6629\ cm^{-1}$ and $^3F_4 \rightarrow {}^3H_6 = 5963\ cm^{-1}$ are slightly different. The lifetime of the $^3F_4$ state is of the order of milliseconds because it is depopulated to the ground state $^3H_6$ by predominantly radiative decay. So the $^3F_4$ state is the storage reservoir and is interesting for laser operation because of its long lifetime. On the other hand, for the 1.48 μm transition, the lifetime of the $^3F_4$ terminal level is higher than that of the initial level. Such a long lifetime compared to that of the $^3H_4$ level makes the $^3H_4 \rightarrow {}^3F_4$ transition self-terminating.

TABLE II. Experimental decay times of the $^3H_4$ and $^3F_4$ energy levels of Tm^{3+} in KGW single crystals as a function of thulium concentration $[Tm^{3+}]$.

$[Tm^{3+}]$	0.1%	1%	3%	5%	7.5%	10%
$\tau(^3H_4(\mu s))$	242	175	94	41	20	8
$\tau(^3F_4(\mu s))$	⋯	1710	1760	1690	1570	1530

IV. CONCLUSIONS

In conclusion, we studied the emission spectra for the 1.48 and 1.84 μm near infrared emissions pumping at 788 nm. From the polarized RT optical absorption measurements we calculated the stimulated emission cross-section using the reciprocity method. The maximum emission cross-sections are $3.0\times10^{-20}\ cm^2$ at 1.838 μm and $1.9\times10^{-20}\ cm^2$ at 1.756 μm for the polarization parallel to the N_m and N_p principal optical directions, respectively. We were therefore able to calculate the optical gain for several population inversion rates and determine the spectral region in which light amplification is possible for future laser experiments using this material for infrared emissions. From the gain versus wavelength, we found a tunability range of more than 300 nm for the $^3F_4 \rightarrow {}^3H_6$ transition. The very long lifetime of the $^3F_4$ energy level of thulium in KGW shows that easy population inversion is expected. This is needed for generating laser radiation. Our promising results encourage us to continue our research into the laser action of thulium in KGW for the 1.84 μm emission.

ACKNOWLEDGMENTS

We gratefully acknowledge financial support from ClCyT under Project Nos. MAT2002-04603-C05-03, FiT-070000-2001-477 and FiT-070000-2002-461, and from CIRIT under Project No. 2001SGR00317. We also acknowledge financial support from MONOCROM S. L.

[1] M. C. Pujol, R. Solé, J. Gavaldà, M. Aguiló, F. Díaz, V. Nikolov, and C. Zaldo, J. Mater. Res. **14**, 3739 (1999).
[2] R. C. Stoneman and L. Esterowitz, Opt. Lett. **16(4)**, 232 (1991).
[3] E. R. Taylor, L. N. Ng, N. P. Sessions, and H. Buerger, J. Appl. Phys. **92**, 112 (2002).
[4] B. M. Antipenko, A. A. Mak, O. B. Raba, K. B. Seiranyan, and T. V. Uvarova, Sov. J. Quantum Electron. **13(4)**, 558 (1983).
[5] G. J. Kintz, R. Allen, and L. Esterowitz. Technical Digest, CLEO'88, OSA paper FB-2 (1988).
[6] A. A. Kaminskii, L. Li, A. V. Butashin, V. S. Mironov, A. A. Pavlyuk, S. N. Bagayev, and K. Ueda, Jpn. J. Appl. Phys., Part 2 **36**, L109 (1997).
[7] S. N. Bagaev, S. M. Vatnik, A. P. Maiorov, A. A. Pavlyuk, and D. V. Plakushchev, Quantum Electron. **30(4)**, 310 (2000).
[8] V. Sudesh and J. A. Piper, IEEE J. Quantum Electron. **36**, 879 (2000).
[9] M. C. Pujol, M. Aguiló, F. Díaz, and C. Zaldo, Opt. Mater. (Amsterdam, Neth.) **13**, 33 (1999).
[10] A. Brenier, C. Pedrini, B. Moine, J. L. Adam, and C. Pledei, Phys. Rev. B **41**, 5364 (1990).
[11] F. Güell, X. Mateos, J. Gavaldà, R. Solé, M. Aguiló, F. Díaz, M. Galan, and J. Massons. Opt. Mat. (accepted).
[12] F. Güell, X. Mateos, R. Solé, J. Gavaldà, M. Aguiló, F. Díaz, and J. Massons. J. Lumin. (accepted).
[13] D. E. McCumber, Phys. Rev. **136**, A954 (1964).
[14] L. Laversenne, C. Goutaudier, Y. Guyot, M. T. Cohen-Adad, and G. Boulon, J. Alloys Compd. **341**, 214 (2002).
[15] K. Ohta, H. Saito, and M. Obara, J. Appl. Phys. **73**, 3149 (1992).
[16] G. Rustad and K. Stenersen, IEEE J. Quantum Electron. **32**, 1645 (1996).
[17] A. Braud, P. Y. Tigreat, J. L. Doualan, and R. Moncorgé, Appl. Phys. B: Lasers Opt. **72**, 909 (2001).
[18] W. Ryba-Romanowski, S. Golab, I. Sokolska, G. Dominiak Dzik, J. Zawadzka, M. Berkowski, J. Fink Finowicki, and M. Baba, Appl. Phys. B: Lasers Opt. **68**, 199 (1999).
[19] S. A. Payne, L. L. Chase, L. K. Smith, W. L. Kway, and W. F. Krupke, IEEE J. Quantum Electron. **28**, 2619 (1992).